

Dynamic Control of Pneumatic Muscle Actuators

Isuru S. Godage*, Yue Chen†, and Ian D. Walker‡

Abstract—Pneumatic muscle actuators (PMA) are easy-to-fabricate, lightweight, compliant, and have high power-to-weight ratio, thus making them the ideal actuation choice for many soft and continuum robots. But so far, limited work has been carried out in dynamic control of PMAs. One reason is that PMAs are highly hysteretic. Coupled with their high compliance and response lag, PMAs are challenging to control, particularly when subjected to external loads. The hysteresis models proposed to-date rely on many physical and mechanical parameters that are difficult to measure reliably and therefore of limited use for implementing dynamic control. In this work, we employ a Bouc-Wen hysteresis modeling approach to account for the hysteresis of PMAs and use the model for implementing dynamic control. The controller is then compared to PID feedback control for a number of dynamic position tracking tests. The dynamic control based on the Bouc-Wen hysteresis model shows significantly better tracking performance. This work lays the foundation towards implementing dynamic control for PMA-powered high degrees of freedom soft and continuum robots.

I. INTRODUCTION

Pneumatic muscle actuators (PMA) are a popular choice for powering soft and continuum robots [1]. Their lightweight design, high compliance and high power-to-weight ratio, combined with the ease of fabrication and customization have fueled their popularity among the researchers and hobbyists alike [1]. Invented in late 50's (also known as McKibben artificial muscles [2]) PMAs have been well studied over the years and commercialized for industrial applications [3]. Based on the same fundamental operation principle, researchers have investigated novel varieties of PMA actuators to generate non-linear and complex deformations beyond the linear (extending or contracting) strain of traditional PMAs [4]. Moreover, the PMA's also laid the foundation for novel types of fluidic muscle actuators, such as fiber-reinforced soft bending actuators [5], now widespread in soft robotics [6].

Unlike the soft bending actuators [5], PMA powered robots, such as multisection continuum arms [7], can operate at much higher pressure levels, and therefore are able to generate higher forces to execute useful tasks in the task-space. The stiffness of PMAs, which is a function of the pressure provided, could be varied within a wider range to attain compliance for environmental interactions and stiffness for supporting body weight during manipulation [8] and locomotion [9]. For instance, the well known OctArm continuum robotic

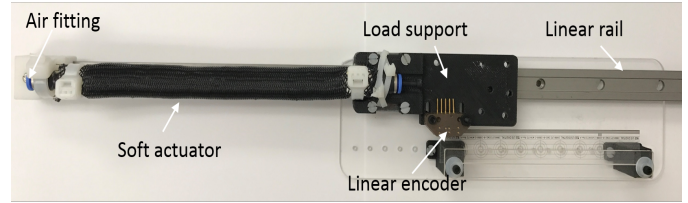


Fig. 1. Pneumatic muscle actuator (PMA) experimental setup, detailing the separate elements.

manipulator, developed at Clemson University by Dr. Walker and the group demonstrated a range of applications including compliant manipulation of fragile objects as well as manipulating and dragging heavy objects [10].

The recent surge in soft robotics and compliant human-friendly robotics have collectively put the spotlight back on compliant actuators such as PMAs [11]. Despite the widespread usage and research conducted on soft and continuum robots, which has spanned over a decade and half, PMA powered robots are still largely confined to laboratory settings with their demonstrated potential untapped. This lag can be attributed to the lack of effective dynamic control schemes developed for such robots for handling the compliance and hysteresis; which essentially leads to better PMA dynamic models. For instance, for systems as complex as a traditional robot manipulator (with 7+ degrees of freedom), the continuum robot state-of-the-art research lags in terms of dynamic control and efficient dynamic models. The latter however has seen significant advancement lately [12].

The overall dynamics of continuum arms heavily depend on the dynamics of PMAs. Yet, most of the dynamic models for continuum robots employ intermediate joint-space variables such length change of PMAs while pressure is being the true controlled variable. In quasi-static conditions, one can consider that the length variation of a PMAs is proportional to pressure. However, because of the hysteresis, this assumption does not hold for dynamic motion, which is a requirement for robots to efficiently operate in the task-space or match the human operation bandwidth in human spaces as co-robots.

Prior work have taken different avenues to model PMAs [13], [14]. Bulk of the work focuses on static or quasi-static models and propose methodologies to systematically derive the models based on physical parameters (such as bladder dimensions) and mechanical properties (i.e., elastic coefficient etc.) of the construction material. However, these properties are difficult to measure reliably, especially when they are heavily coupled to one another during PMA development. Thus, models have been limited to theoretical studies with inadequate

* School of Computing, DePaul University, Chicago, IL 60604. email: igodage@depaul.edu. † Dept. of Mechanical Engineering, University of Arkansas, Fayetteville, AR 72701. ‡ Dept. of Electrical and Computer Engineering, Clemson University, SC 29634.

This work is supported in part by the National Science Foundation grant IIS-1718755.

experimental testing, notably related to dynamics. Relatively low attention has been paid for developing hysteresis models for PMAs [14] and limited work has shown experimental evaluation under external load [15]. Also, tests carried out to-date were also limited to tracking signals of bandwidth less than 0.5 Hz. The authors introduced a variant of Bouc-Wen hysteresis model for PMAs in [16]. The method relies on experimental characterization to identify the actuator specific dynamic behavior and hysteresis. This approach is particularly suitable for accounting for varying performance of PMAs due to complex and nonlinear interactions of materials and variations of the fabrication method. Utilizing the Bouc-Wen hysteresis model, the authors have shown that the model is able to correctly simulate the hysteretic behavior of PMAs individually as well as a continuum section (where three PMAs are bundled together for generating spatial bending).

This work extends the contribution reported in [16] and presents the initial results on the implementation of dynamic control for PMA's based on the Bouc-Wen hysteresis model. The paper is organized as follows. Section II details the experimental setup, the dynamic model and the details of system identification process and the controller design. Section III presents the experimental results and compares the kinematic feedback control performance to the computed torque control output that utilizes the Bouc-Wen hysteresis model followed by the concluding remarks in Section IV.

II. MATERIALS AND METHODS

A. Experimental Setup

Figure 1 shows the experimental setup consisting of the prototype PMA, high resolution (2000 quadrature counts per inch) linear optical encoder, variable external load support, and air supply to the PMA. The PMA construction is similar to the one detailed in [16]. The bladder is a silicone tube of 12 mm diameter with 1.5 mm wall thickness, enclosed within a 14 mm diameter Nylon braided mesh, and mounted on 4 mm pneumatic union connectors at either end. The PMA has 170 mm unactuated length (l_0) and 85 mm steady state extension (calculated from 10 measurements taken 100 s after applying the pressure step) at 0.4 MPa. The PMA has a 0.022 kg mass where the moving carriage has 0.045 kg mass. The PMA is attached between an immobile base and the low-friction moving carriage (McMasterCarr part # 6250K42), mounted on a linear rail (McMasterCarr part # 6250K3), to ensure that the PMA changes length axially. The air pressure to the PMA is controlled by a digital proportional pressure regulator (Pneumax 171E2N.T.D.0005S) that is controlled via an analog, 0-10 V (maps to 0-0.9 MPa) voltage input provided through a National Instruments PCI-6703 data acquisition interface card. The quadrature encoder pulses are counted using a CONTEC CNT-3208M-PE timer/counter interface card. The interface cards are mounted on a Matlab Simulink Realtime target machine and controlled directly from a Simulink model on a host computer and solved using an ODE14X solver at 1 kHz. This high update rate ensures minimal delay and accurate dynamic control performance.

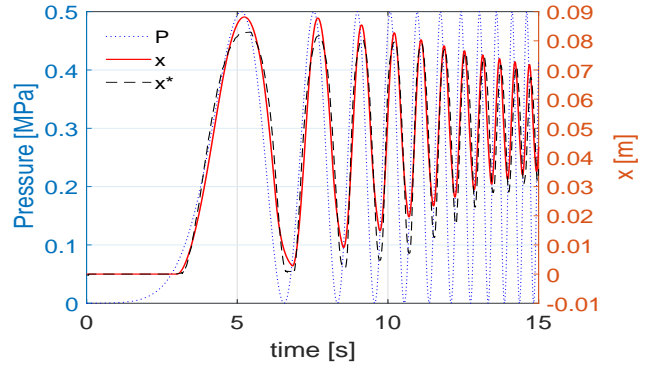


Fig. 2. The plot of the sinusoidal chirp input pressure signal, system response to the input signal, and the simulated system response with the use of optimal Bouc-Wen shape coefficients.

B. Dynamic Model with Hysteresis

Schematic diagram of the dynamic system model we used in this work is shown in Fig. 3. The carriage mass, M , to which the free end of the PMA is considered as a load on the system. Similar to [16], using the Lagrangian mechanical principles, the PMA dynamic model can be derived as a single degree of freedom system given by

$$(M + m) \ddot{x} + (M + m)g + K_e x + z = Ap \quad (1)$$

$$\dot{z} = \dot{x}[\alpha - \{\beta \text{sgn}(\dot{x}z) + \gamma\}|z|] \quad (2)$$

where M , m , K_e , g , and x are the variable load mass, PMA mass, PMA bladder linear elastic stiffness, gravitational acceleration, and PMA length change. For an in-depth treatment of the equation of motion (EoM) derivation, the readers are referred to [16]. $\alpha > 0 \in \mathbb{R}$, $\beta > 0 \in \mathbb{R}$, and $\gamma \in \mathbb{R}$ are dimensionless Bouc-Wen hysteresis loop control parameters. A is the cross-section area of the PMA and p is the supplied pressure (joint-space variable).

The shape of the hysteresis curve can be matched to that of the experimental results by finding the appropriate values for α , β , and γ . To realize this, we apply the PMA with a signal of varying frequency to ensure to capture as much dynamic response information as possible in order to model the system well in faster motion. The PMA was provided with a 0.5 MPa sinusoidal chirp signal of frequencies from 0.1 Hz to 3 Hz for a 15 s duration and the input pressure signal

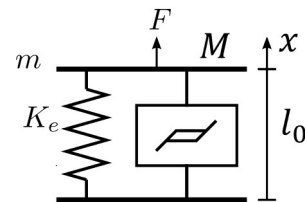


Fig. 3. PMA model with the Bouc-Wen hysteresis block.

and the system response, x' , were recorded. This experiment is repeated 10 times and the average system response is computed by taking the mean response at each time step. The frequency range and the variation ensure that both quasi-static (low frequency), transient, and dynamic behavior of the system are captured. The experimentally recorded data (x'), are then used to identify the Bouc-Wen hysteresis shape coefficients. To achieve this, we implemented the EoM, given by (1) and (2), in Matlab Simulink and defined the cost function, $c \in \mathbb{R}$, given by

$$c(\alpha, \beta, \gamma, d, K_e, p_{dz}) = \text{RMS} \sum_{\forall t} (x - x') \quad (3)$$

where t denotes a specific time instance when we measured the experimental data and x is the simulated system response. To derive the cost function for the entire simulation, we compute the vector of differences of the simulated and experimental data for each time sample and then take the root mean square (RMS) value of this array. In addition to hysteresis shape parameters, we include the system damping (d), elastic coefficient (K_e), and the PMA dead zone (p_{dz}) as parameters to be modeled for the setup shown in Fig. 1. The reason for including the latter parameters is that it is challenging to experimentally measure them reliably in dynamic motion.

We then employed the Matlab global search functionality and ran a constrained optimization routine (using 'fmincon') until we find the optimal Bouc-Wen hysteresis shape parameters. Figure 2 also shows the simulated response, obtained from (1), using the optimal Bouc-Wen shape parameters given by $\alpha = 23.705$, $\beta = 1.7267$, and $\gamma = -42.593$ where as $d = 155.76$, $K_e = 624.78$, and $p_{dz} = 66.922$ kPa. The optimized numerical model's output is then plotted alongside the experimental data. It can be seen that the numerical model captures the system dynamics, both steady state and dynamics, well overall.

III. EXPERIMENTAL RESULTS

The dynamic model is then used to implement the control system shown in Fig. 4 which includes the standard joint-space feedback (kinematic) PID controller and the computed

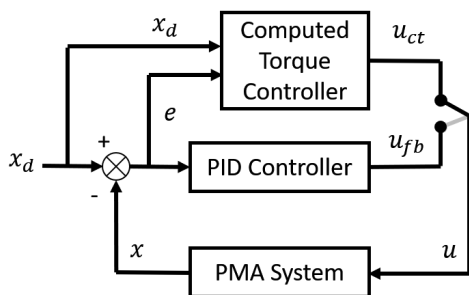


Fig. 4. Computed torque controller and the standard joint-space PID controller.

torque controller [17] utilizing the dynamic model described in Section II-B. The controller is implemented in Matlab Simulink Realtime and switched between the two for assessing the control performance. In the Simulink Realtime model, the inner control loop was run at 100 Hz where the input signals to the pressure regulator was run at 20 Hz. This low outer control loop ensures that the digital pressure regulator bandwidth is matched without driving the inner pressure control loop unstable. As the load, we use a 500 g weight and we erected the experimental setup so that the gravity induced weight is toward the PMA extension (downwards). This prevents the PMA from buckling under the load as here, there is no constraining mechanism like the one reported in [16].

Then we applied the sinusoidal position tracking signal given by

$$x_d = 0.005 + 0.0225 \sin(2\pi ft) \quad (4)$$

where f is the frequency of the signal. Note the 0.005 m bias we applied to the tracking signal to compensate initial position offset caused by the applied external load.

The performance of PID feedback control and the proposed computed torque controller that uses the Bouc-Wen hysteresis model was then evaluated. The sub-figures under each test shown in Fig. 5 compare the position tracking error for both PID control and computed torque controllers. Figure 5-a shows the controller performance results for $f = 0.5$ Hz signal tracking. Note that 0.5 Hz is relatively fast signals to track in comparison to prior work on PMA control which typically include frequencies less than 0.5 Hz. The computed torque controller performance is superior to PID controller particularly in phase response. This is significant, especially when comparing the inherent lag present in PMAs. For instance, the system response for the characterization signal shown in Fig. 2, exhibit this phase lag of the output. This lag is reflected on the PID controller output and becomes a significant factor when tracking high frequency signals such as 1 Hz (Fig. 5-b). This system delay, to a lesser degree, also affects the computed torque controller but yet shows better tracking performance where PID controller fails to maintain the pace of tracking. Note that the dynamic controlled response exhibits about 10% overshoot but quickly corrects quickly to follow the falling edge accurately. We then pushed our controllers to track a 2 Hz signal and the results are compared in Fig. 5-c. Here, both controllers were unable to track the signal well, although the computed torque controller output was better overall and within an acceptable, less than 180° , phase lag and overall tracking amplitude profile. Whereas the PID control output was 180° out of phase. Hence, the proposed work demonstrates strong potential to be useful in realizing PMA-powered multisection continuum arm dynamic control towards applications in human spaces.

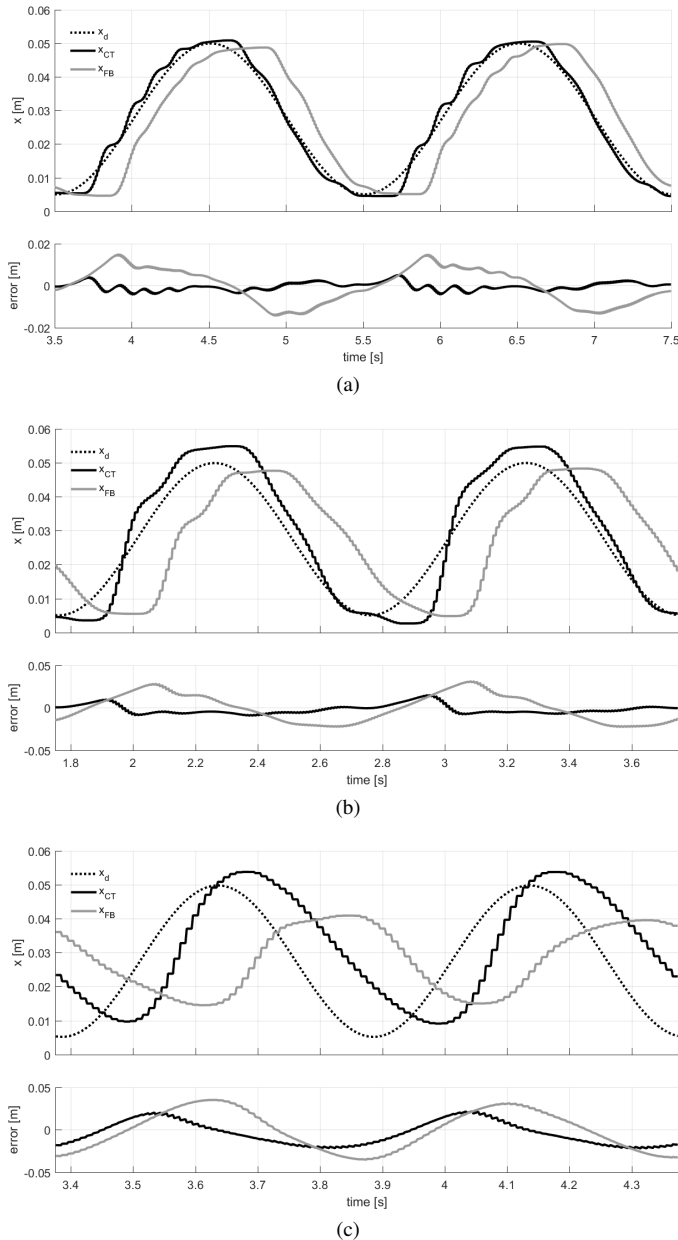


Fig. 5. Computed torque controller and the standard joint-space PID controller performance comparison, (a) 0.5 Hz frequency, (b) 1.0 Hz, and (c) 2.0 Hz. The plots below each experiments shows the tracking error. x_d is the desired tracking signal, x_{FB} is the PID controller output, and x_{CT} is the computed torque controller output.

IV. CONCLUSIONS AND FUTURE WORK

Pneumatic muscle actuators (PMAs) are the choice of many, researchers and hobbyists alike for powering soft and continuum robots. PMA desirable features include inherent compliance and high power-to-weight ratio. PMA operation is highly hysteretic, posing challenges in controlling them, particularly in highly dynamic applications. Consequently, the soft and continuum robots so far have been limited to teleoperation (open-loop control) or kinematic (slow motions) control thus limiting their application potential. We proposed a dynamic control scheme for PMAs, which is based on the

dynamic model previously proposed by the authors, where hysteresis is modeled via a Bouc-Wen hysteresis model. The work compared the dynamic control performance to a PID feedback controller for a number of dynamic position tracking tests on a PMA with external loading. The results showed that the proposed dynamic controller is capable of tracking the dynamic signals better. We plan to extend the proposed dynamic control approach to the continuum arm reported in [12] in manipulation tasks in human spaces.

REFERENCES

- [1] F. Daerden and D. Lefeber, "Pneumatic artificial muscles: actuators for robotics and automation," *European journal of mechanical and environmental engineering*, vol. 47, no. 1, pp. 11–21, 2002.
- [2] B. Tondu and P. Lopez, "Modeling and control of mckibben artificial muscle robot actuators," *IEEE control systems*, vol. 20, no. 2, pp. 15–38, 2000.
- [3] F. F. Muscle, "Festo brochure fluidic muscle," Also available at: <http://www.festo.com/cat/nl-be/be/data/doc/engb/PDF/EN/DMSP-MAS EN.PDF>.
- [4] G. Krishnan, J. Bishop-Moser, C. Kim, and S. Kota, "Kinematics of a generalized class of pneumatic artificial muscles," *Journal of Mechanisms and Robotics*, vol. 7, no. 4, p. 041014, 2015.
- [5] P. Polygerinos, Z. Wang, J. T. Overvelde, K. C. Galloway, R. J. Wood, K. Bertoldi, and C. J. Walsh, "Modeling of soft fiber-reinforced bending actuators," *IEEE Transactions on Robotics*, vol. 31, no. 3, pp. 778–789, 2015.
- [6] M. T. Tolley, R. F. Shepherd, B. Mosadegh, K. C. Galloway, M. Wehner, M. Karpelson, R. J. Wood, and G. M. Whitesides, "A resilient, untethered soft robot," *Soft robotics*, vol. 1, no. 3, pp. 213–223, 2014.
- [7] I. S. Godage, D. T. Branson, E. Guglielmino, G. A. Medrano-Cerda, and D. G. Caldwell, "Shape function-based kinematics and dynamics for variable length continuum robotic arms," in *Robotics and Automation (ICRA), 2011 IEEE International Conference on*. IEEE, 2011, pp. 452–457.
- [8] I. D. Walker, D. M. Dawson, T. Flash, F. W. Grasso, R. T. Hanlon, B. Hochner, W. M. Kier, C. C. Pagano, C. D. Rahn, and Q. M. Zhang, "Continuum robot arms inspired by cephalopods," in *Unmanned Ground Vehicle Technology VII*, vol. 5804. International Society for Optics and Photonics, 2005, pp. 303–315.
- [9] I. S. Godage, T. Nanayakkara, and D. G. Caldwell, "Locomotion with continuum limbs," in *Intelligent Robots and Systems (IROS), 2012 IEEE/RSJ International Conference on*. IEEE, 2012, pp. 293–298.
- [10] W. McMahan, V. Chitrakaran, M. Csencsits, D. Dawson, I. D. Walker, B. A. Jones, M. Pritts, D. Diemno, M. Grissom, and C. D. Rahn, "Field trials and testing of the octarm continuum manipulator," in *Robotics and Automation, 2006. ICRA 2006. Proceedings 2006 IEEE International Conference on*. IEEE, 2006, pp. 2336–2341.
- [11] D. Rus and M. T. Tolley, "Design, fabrication and control of soft robots," *Nature*, vol. 521, no. 7553, p. 467, 2015.
- [12] I. S. Godage, G. A. Medrano-Cerda, D. T. Branson, E. Guglielmino, and D. G. Caldwell, "Dynamics for variable length multisection continuum arms," *The International Journal of Robotics Research*, vol. 35, no. 6, pp. 695–722, 2016.
- [13] D. Reynolds, D. Repperger, C. Phillips, and G. Bandry, "Modeling the dynamic characteristics of pneumatic muscle," *Annals of biomedical engineering*, vol. 31, no. 3, pp. 310–317, 2003.
- [14] T. D. C. Thanh and K. K. Ahn, "Nonlinear pid control to improve the control performance of 2 axes pneumatic artificial muscle manipulator using neural network," *Mechatronics*, vol. 16, no. 9, pp. 577–587, 2006.
- [15] C.-P. Chou and B. Hannaford, "Measurement and modeling of mckibben pneumatic artificial muscles," *IEEE Transactions on robotics and automation*, vol. 12, no. 1, pp. 90–102, 1996.
- [16] I. S. Godage, D. T. Branson, E. Guglielmino, and D. G. Caldwell, "Pneumatic muscle actuated continuum arms: Modelling and experimental assessment," in *Robotics and Automation (ICRA), 2012 IEEE International Conference on*. IEEE, 2012, pp. 4980–4985.
- [17] R. M. Murray, *A mathematical introduction to robotic manipulation*. CRC press, 2017.